

Joint Beam Training and Data Transmission Design for Covert Millimeter-Wave Communication

Jiayu Zhang, Min Li, Shihao Yan, Chunshan Liu, Xihan Chen, Minjian Zhao and Philip Whiting

Abstract—Covert communication prevents legitimate transmission from being detected by a warden while maintaining certain covert rate at the intended user. Prior works have considered the design of covert communication over conventional low-frequency bands, but few works so far have explored the higher-frequency millimeter-wave (mmWave) spectrum. The directional nature of mmWave communication makes it attractive for covert transmission. However, how to establish such directional link in a covert manner in the first place remains as a significant challenge. In this paper, we consider a covert mmWave communication system, where legitimate parties Alice and Bob adopt beam training approach for directional link establishment. Accounting for the training overhead, we develop a new design framework that jointly optimizes beam training duration, training power and data transmission power to maximize the effective throughput of Alice-Bob link while ensuring the covertness constraint at warden Willie is met. We further propose a dual-decomposition successive convex approximation algorithm to solve the problem efficiently. Numerical studies demonstrate interesting tradeoff among the key design parameters considered and also the necessity of joint design of beam training and data transmission for covert mmWave communication.

Index Terms—Beam alignment, beam training, covert communication, millimeter-wave communications, training-throughput tradeoff.

I. INTRODUCTION

Covert communication [1], also known as low-probability-of-detection (LPD) communication [2], has emerged as a new security paradigm in wireless systems. Different from conventional physical-layer security methods, covert communication aims to hide the very existence of legitimate transmission from an adversary while maintaining a certain covert rate at the intended user. It therefore achieves a stronger security and privacy level, which is highly desired in the emerging 5G/IoT systems and advanced military networks [3], [4].

Consider a classic covert communication setup, where Alice wishes to send message to Bob over a wireless channel, while ensuring that the probability of the transmission being detected by a warden Willie is small (i.e., a covertness constraint at Willie). For an additive white Gaussian noise (AWGN) channel, Bash *et al.* [2] established that Alice can only send $\mathcal{O}(\sqrt{n})$ covert bits to Bob over n channel uses. This square-root law has later been shown to also hold for a binary symmetric channel [5]

Jiayu Zhang, Min Li, Xihan Chen and Minjian Zhao are with College of Information Science and Electronic Engineering, Zhejiang University, Hangzhou, 310027, China (e-mail: {11731056, min.li, chenxihan, mjzhao}@zju.edu.cn).

Shihao Yan and Philip Whiting are with School of Engineering, Macquarie University, Sydney, NSW 2109, Australia (e-mail: {shihao.yan, philip.whiting}@mq.edu.au).

Chunshan Liu is with School of Communication Engineering, Hangzhou Dianzi University, Hangzhou, 310018, China (e-mail: chunshan.liu@hdu.edu.cn).

and a broader class of discrete memoryless channels [6]. However, this square-root result can be further improved, for instance, by the use of an additional jammer to facilitate Alice's transmission [7]. Note such scaling-law results are obtained for sufficiently large n .

Yan *et al.* [8] instead considered a delay-intolerant setup and studied the impact of finite n on the covert communication performance. The optimality of Gaussian signalling has been then analyzed in delay-intolerant covert communications [9]. Various other practical constraints, such as channel uncertainty [10], [11] and noise uncertainty [12] have also been modeled and investigated in covert communications. In addition, more complicated scenarios that involve artificial noise [13], multi-antenna nodes [14]–[18], full-duplex nodes [19] and relay-assisted transmission [20]–[22] have also been considered.

The above works focused on the design of covert transmission over conventional low-frequency bands. Compared to these frequency bands, millimeter-wave band has much more under-utilized spectrum and has now been put forward as an important means to expand the capacity for mobile communications [23], [24]. Due to its unfavorable propagation characteristics (such as high path loss and limited scattering), mmWave communication would heavily rely on beamforming transmission to ensure reliable links. The directional nature of the communication link makes it inherently suitable for covert transmission, because it is much more challenging for an adversary to overhear all of the communication.

While the potential of mmWave covert communication is conceivable, fundamental understanding and design guidelines for such system are still lacking. Related studies are scant except [25], [26], to the best of our knowledge. Reference [25] introduced a conceptual framework of mmWave soldier-to-soldier covert communications and discussed a few challenges at the physical layer and medium access control layer. However, it neither considered beamforming design that is crucial for the system nor provided rigorous quantification of the covertness level the framework can fundamentally achieve. Reference [26] considered a covert mmWave communication system, where Alice deploys dual independent antenna arrays, with one to form a beam towards Bob for covert data transmission and the other to form another beam towards Willie for jamming transmission. The outage probability and optimal covert rate of Alice-Bob link were characterized. However, this work only focused on the data transmission phase and did not address how the Alice-Bob directional link is established in the first place and whether or not the establishment of such link would require additional communication that might be detected by

For the scenario described, we further assume a frame-slotted communication between Alice and Bob. As illustrated in Fig. 1, each frame has n symbols in total (e.g., on the order of channel coherence time) and is further divided into a beam alignment (BA) phase that consists of n_a symbols and a data transmission (DT) phase of $n - n_a$ symbols. In the BA phase, Alice and Bob jointly train transmit/receive beam pairs from pre-designed codebooks so as to determine the best beam pair that is then used for the subsequent DT phase. Both BA and DT phases should be carefully designed so that the directional link between Alice and Bob is sufficiently good and the probability of detection of communication at Willie is kept at the covertness level required.

In what follows, we first elaborate the signalling model for communication between Alice and Bob and then define the binary hypothesis detection problem at Willie.

B. Signalling Model for Beam Alignment and Data Transmission Between Alice and Bob

We assume that Alice and Bob adopt an exhaustive-search (ES) strategy for beam training [27]. Specifically, let $\mathcal{C}_a = \{\bar{\mathbf{w}}_{l_a} \in \mathbb{C}^{N_a \times 1}, l_a \in [1 : L_a]\}$ be a set of L_a unit-norm beams that jointly cover the Angle of Departure (AoD) interval at Alice, while $\mathcal{C}_b = \{\bar{\mathbf{f}}_{l_b} \in \mathbb{C}^{N_b \times 1}, l_b \in [1 : L_b]\}$ be a set of L_b unit-norm beams that jointly cover the Angle of Arrival (AoA) interval at Bob. The entire training codebook is then formed by considering all possible $L = L_a L_b$ Alice/Bob beam pairs, i.e., $\mathcal{C} = \{(\mathbf{w}, \mathbf{f}) : \mathbf{w} \in \mathcal{C}_a, \mathbf{f} \in \mathcal{C}_b\}$.

For each $(\mathbf{w}_l, \mathbf{f}_l) \in \mathcal{C}$, Alice sends a pilot sequence via beam \mathbf{w}_l , while Bob performs an output measurement via beam \mathbf{f}_l . The output signal at Bob is given by

$$\mathbf{y}_l^p = \sqrt{P_a} \mathbf{f}_l^\dagger \mathbf{H}_{ab} \mathbf{w}_l \mathbf{x}^p + \mathbf{z}_b^p, \quad l \in [1 : L], \quad (1)$$

where P_a is the transmit power for beam training at Alice, $\mathbf{x}^p \in \mathbb{C}^{n_p \times 1}$ denotes the pilot sequence with $\|\mathbf{x}^p\|_2^2 = n_p$, $\mathbf{H}_{ab} \in \mathbb{C}^{N_b \times N_a}$ denotes the channel between Alice and Bob, $\mathbf{z}_b^p \in \mathbb{C}^{n_p \times 1}$ is the equivalent channel noise vector after received beamforming, whose elements are i.i.d. as $z_{b,i}^p \sim \mathcal{CN}(0, \sigma_b^2)$. Assuming that the beam pairs in ES are allocated with equal training budget, we thus have $n_p = n_a/L$.

In particular, we consider single-path light-of-sight (LOS) channel between Alice and Bob, and thus channel \mathbf{H}_{ab} can be specialized to

$$\mathbf{H}_{ab} = \gamma_{ab} \mathbf{u}(\phi) \mathbf{v}^\dagger(\psi), \quad (2)$$

where γ_{ab} is the channel coefficient, while $\mathbf{u}(\phi) \in \mathbb{C}^{N_b \times 1}$ and $\mathbf{v}(\psi) \in \mathbb{C}^{N_a \times 1}$ are the steering vectors corresponding to AoA ϕ and AoD ψ that are defined as

$$\mathbf{u}(\phi) = [1, e^{j2\pi \frac{d}{\lambda} \sin(\phi)}, \dots, e^{j2\pi \frac{d}{\lambda} (N_b-1) \sin(\phi)}]^T, \quad (3)$$

$$\mathbf{v}(\psi) = [1, e^{j2\pi \frac{d}{\lambda} \sin(\psi)}, \dots, e^{j2\pi \frac{d}{\lambda} (N_a-1) \sin(\psi)}]^T, \quad (4)$$

respectively, with λ being the wave-length and d being the antenna spacing. Under this model and when $(\mathbf{w}_l, \mathbf{f}_l)$ beam pair is trained, the effective channel in (1) is specialized to

$$h_l = \gamma_{ab} \mathbf{f}_l^\dagger \mathbf{u}(\phi) \mathbf{v}^\dagger(\psi) \mathbf{w}_l, \quad (5)$$

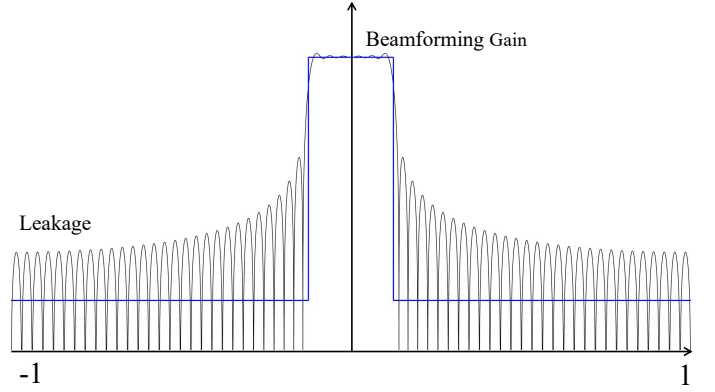


Fig. 2. An illustration of the generalized flat-top beam pattern adopted.

with beamforming gain

$$\begin{aligned} G_l &\triangleq |\mathbf{f}_l^\dagger \mathbf{u}(\phi) \mathbf{v}^\dagger(\psi) \mathbf{w}_l|^2 \\ &= F_l(\phi) W_l(\psi), \end{aligned} \quad (6)$$

where $W_l(\psi) \triangleq |\mathbf{v}^\dagger(\psi) \mathbf{w}_l|^2$ is the transmit beamforming gain along AoD ψ at Alice side, while $F_l(\phi) \triangleq |\mathbf{f}_l^\dagger \mathbf{u}(\phi)|^2$ is the receive beamforming gain along AoA ϕ at Bob side.

We also consider that each of the beams trained has uniform gain within its intended coverage interval (i.e., its mainlobe) and constant small leakage outside the mainlobe (as illustrated in Fig. 2) as in [31]. This slightly generalizes the commonly used flat-top beam model and is useful to capture the side-lobe leakage of non-ideal beams in practice. Moreover, assuming that all Alice (Bob) beams have equal-size non-overlapping mainlobes that jointly cover the AoD range Ψ (resp. AoA Φ), so Alice (Bob) beamforming gain can then be represented as

$$W_l(\psi) = \begin{cases} W_a, & \text{if } \psi \in \Psi_{\mathbf{w}_l} \\ w_a, & \text{otherwise} \end{cases} \quad (7)$$

and

$$F_l(\phi) = \begin{cases} F_b, & \text{if } \phi \in \Phi_{\mathbf{f}_l} \\ f_b, & \text{otherwise} \end{cases}, \quad (8)$$

respectively, where $\Psi_{\mathbf{w}_l}$ and $\Phi_{\mathbf{f}_l}$ denote the mainlobe interval (in the \sin domain) of beam \mathbf{w}_l and \mathbf{f}_l , respectively, and $W_a \gg w_a$, $F_b \gg f_b$.

With the above assumptions, the output signal of (1) at Bob is then specialized to

$$\mathbf{y}_l^p = \gamma_{ab} \sqrt{P_a G_l} \mathbf{x}^p + \mathbf{z}_b^p, \quad (9)$$

where G_l is drawn from the set $\{W_a F_b, w_a F_b, W_a f_b, w_a f_b\}$, which depends on how well the l th beam pair aligns with the underlying channel.

In addition, Alice and Bob are assumed to share the pilot sequences used for beam training beforehand. Given output measurement \mathbf{y}_l^p and the known pilot sequence \mathbf{x}^p , Bob can then further form match-filtered outputs as

$$\tilde{\mathbf{y}}_l^p = (\mathbf{x}^p)^\dagger \mathbf{y}_l^p \quad (10)$$

$$= n_p \gamma_{ab} \sqrt{P_a G_l} + (\mathbf{x}^p)^\dagger \mathbf{z}_b^p, \quad l \in [1 : L]. \quad (11)$$

The beam pair $(\mathbf{w}_{l_{ES}}, \mathbf{f}_{l_{ES}})$ as leading to the strongest match-filtered output is then chosen the one used for subsequent data

transmission, where \hat{l}_{ES} is given by

$$\hat{l}_{\text{ES}} = \arg \max_{l \in [1:L]} |\hat{y}_l^p|. \quad (12)$$

In this way, during the DT phase, the Alice-to-Bob channel input-output relationship is represented by

$$\mathbf{y}_b^d = \gamma_{ab} \sqrt{P_d G_d} \mathbf{x}^d + \mathbf{z}_b^d, \quad (13)$$

where $\mathbf{x}^d \in \mathbb{C}^{(n-n_a) \times 1}$ is the input data vector with i.i.d. elements $\sim \mathcal{CN}(0, 1)$, P_d is the transmit power for data communication, $G_d = G_{\hat{l}_{\text{ES}}}$ with \hat{l}_{ES} as in (12), $\mathbf{z}_b^d \in \mathbb{C}^{(n-n_a) \times 1}$ noise vector with i.i.d. elements $\sim \mathcal{CN}(0, \sigma_b^2)$ and \mathbf{y}_b^d is the output signal at Bob.

It is clear that the beamforming gain G_d in (13) takes only one of $\{W_a F_b, W_a f_b, w_a F_b, w_a f_b\}$, which depends on the beam alignment performance via ES beam training. Motivated by this, we introduce a notion of average effective throughput

$$\bar{T} = \left(1 - \frac{n_a}{n}\right) \mathbb{E} \left\{ \log \left(1 + \frac{P_d |\gamma_{ab}|^2}{\sigma_b^2} G_d \right) \right\}, \quad (14)$$

to measure the average performance of the Alice-Bob data link, which explicitly takes into account the impact of beam alignment overhead and accuracy on the subsequent data communication. Unless otherwise specified, the log function takes base 2.

C. Binary Detection Problem at Willie

In order to determine the presence of Alice-to-Bob covert communication, Willie needs to distinguish the following two hypotheses

$$\begin{cases} \mathcal{H}_0 : \mathbf{y}_w = \mathbf{z}_w \\ \mathcal{H}_1 : \mathbf{y}_w = \mathbf{s} + \mathbf{z}_w \end{cases} \quad (15)$$

where all $\mathbf{y}_w, \mathbf{s}, \mathbf{z}_w \in \mathbb{C}^{n \times 1}$. Note that \mathcal{H}_0 denotes the null hypothesis where Alice has not communicated with Bob and thus only channel noise vector \mathbf{z}_w (with i.i.d. elements $\sim \mathcal{CN}(0, \sigma_w^2)$) is observed, while \mathcal{H}_1 denotes the alternative hypothesis where Alice has communicated with Bob and thus some information leakage superimposed on channel noise is observed.

Under \mathcal{H}_1 , to be more specific, considering that the Alice-to-Willie link is also in LOS, the resultant channel is then represented as

$$\mathbf{h}_{aw} = \gamma_{aw} \mathbf{v}^\dagger(\psi_{aw}), \quad (16)$$

where ψ_{aw} and γ_{aw} are the associated AoD and channel coefficient, respectively. The signal vector i.e., \mathbf{s} at Willie is thus formed by two parts: The first n_a symbols (i.e., $\mathbf{s}_{[1:n_a]}$) are the signals at Willie when Alice and Bob perform beam training

$$\begin{aligned} \mathbf{s}_{[(l-1)*n_p+1:l*n_p]} &= \sqrt{P_a} \mathbf{h}_{aw} \mathbf{w}_l \mathbf{x}^p \\ &= \begin{cases} \gamma_{aw} \sqrt{P_a} \bar{W}_a \mathbf{x}^p, & \text{if } \psi_{aw} \in \Psi_{\mathbf{w}_l} \\ \gamma_{aw} \sqrt{P_a} w_a \mathbf{x}^p, & \text{otherwise,} \end{cases} \end{aligned} \quad (17)$$

while the rest are the signals at Willie when Alice and Bob perform data transmission:

$$\mathbf{s}_{[n_a+1:n]} = \sqrt{P_d} \mathbf{h}_{aw} \mathbf{w}_{\hat{l}_{\text{ES}}} \mathbf{x}^d. \quad (18)$$

Given \mathbf{s} , Willie makes a binary decision (\mathcal{D}_1 or \mathcal{D}_0) that infers whether Alice's transmission is present or not. Consider equal a priori probability of \mathcal{H}_0 and \mathcal{H}_1 . To measure the detection performance of Willie, we adopt the total detection error probability ξ , which is defined as

$$\xi = \alpha + \beta, \quad (19)$$

where $\alpha \triangleq \Pr(\mathcal{D}_1 | \mathcal{H}_0)$ denotes the false alarm rate, $\beta \triangleq \Pr(\mathcal{D}_0 | \mathcal{H}_1)$ denotes the missed detection rate. Let ξ^* be the minimum error probability Willie can achieve by using an optimal detector.

Our ultimate goal is thus to develop appropriate Alice-to-Bob beam training and data transmission design so as to maximize \bar{T} for Alice-Bob link, while enforcing that $\xi^* \geq 1 - \epsilon$ at Willie for a covertness level $\epsilon > 0$ required. Towards this end, in what follows, we shall first characterize Alice-Bob \bar{T} and Willie's detection performance as a function of key system parameters (including training duration n_a , transmit power P_a and P_d for BA and DT), and then propose a joint optimized design of BA and DT for the covert communication studied.

III. JOINT OPTIMIZATION OF BEAM ALIGNMENT AND DATA TRANSMISSION FOR COVERT MMWAVE COMMUNICATION

A. Characterization of \bar{T} for Alice-Bob Link

For the Alice-Bob link, recall from (14) that the average effective throughput \bar{T} crucially depends on the statistical property of beamforming gain G_d after beam training. In particular, $G_d = W_a F_b$ when there is perfect beam alignment, while G_d takes a much smaller gain from the set $\{W_a f_b, w_a F_b, w_a f_b\}$ if there is one-sided or two-sided misalignment.

To quantify \bar{T} , we introduce the following probability of successful alignment through ES beam training

$$p_{\text{align}} \triangleq \Pr\{\hat{l}_{\text{ES}} = l_{\text{opt}}\}, \quad (20)$$

where $l_{\text{opt}} = \arg \max_{l \in [1:L]} |\mathbf{f}_l^\dagger \mathbf{u}(\phi) \mathbf{v}^\dagger(\psi) \mathbf{w}_l|^2$ is the index of the optimal beam pair that leads to the largest beamforming gain. Considering the facts that beamforming gain is much larger under perfect alignment and that we ought to achieve high p_{align} , we can approximate \bar{T} as

$$\bar{T} \approx \left(1 - \frac{n_a}{n}\right) \log \left(1 + \frac{P_d |\gamma_{ab}|^2}{\sigma_b^2} W_a F_b \right) p_{\text{align}} \quad (21)$$

by dropping the marginal throughput contribution in the case of misalignment for the sake of tractability.

We now further analyze p_{align} . Without loss of optimality and for notational convenience, $l_{\text{opt}} = 1$ is assumed. Based on the ES beam training (12), p_{align} can be represented as

$$\begin{aligned} p_{\text{align}} &= \Pr\{\hat{l}_{\text{ES}} = l_{\text{opt}}\} \\ &= \Pr\{|\hat{y}_1^p| > \max\{|\hat{y}_2^p|, |\hat{y}_3^p|, \dots, |\hat{y}_N^p|\}\} \end{aligned} \quad (22)$$

$$= 1 - \Pr\{|\hat{y}_1^p| \leq \max\{|\hat{y}_2^p|, |\hat{y}_3^p|, \dots, |\hat{y}_N^p|\}\} \quad (23)$$

$$= 1 - \Pr\{T_1 \leq \max\{T_2, T_3, \dots, T_L\}\}, \quad (24)$$

where we have defined normalized statistics

$$T_l = \frac{|\tilde{y}_l^p|^2}{\frac{\sigma_w^2}{2} n_p}, \quad l \in [1 : L]. \quad (25)$$

Let $\chi_k^2(\lambda)$ denote a noncentral chi-squared distribution with degrees of freedom (DoFs) k and noncentral parameter λ . To derive useful properties of p_{align} , we introduce the following lemma.

Lemma 1: The normalized statistics defined all follow noncentral chi-squared distribution with DoFs $k = 2$ and with noncentral parameter drawn from the set $\{\lambda_A, \lambda_B, \lambda_C, \lambda_D\}$ defined as:

$$\lambda_A = \frac{2|\gamma_{ab}|^2 n_p P_a W_a F_b}{\sigma_b^2}, \quad \lambda_B = \frac{2|\gamma_{ab}|^2 n_p P_a w_a F_b}{\sigma_b^2}, \quad (26)$$

$$\lambda_C = \frac{2|\gamma_{ab}|^2 n_p P_a W_a f_b}{\sigma_b^2}, \quad \lambda_D = \frac{2|\gamma_{ab}|^2 n_p P_a w_a f_b}{\sigma_b^2}. \quad (27)$$

Specifically, $T_1 \sim \chi_2^2(\lambda_A)$, while among $\{T_2, T_3, \dots, T_L\}$, $(L_a - 1)$ variables follow $\chi_2^2(\lambda_B)$, $(L_b - 1)$ variables follow $\chi_2^2(\lambda_C)$ and $(L_a - 1)(L_b - 1)$ variables follow $\chi_2^2(\lambda_D)$.

Proof: Following (11), T_l of (25) is represented by

$$T_l = \frac{|\tilde{y}_l^p|^2}{\frac{\sigma_w^2}{2} n_p} = \frac{|n_p \gamma_{ab} \sqrt{P_a G_l} + (\mathbf{x}^p)^\dagger \mathbf{z}_b^p|^2}{\frac{\sigma_w^2}{2} n_p} \quad (28)$$

$$= \left| \gamma_{ab} \sqrt{\frac{n_p P_a G_l}{\frac{\sigma_w^2}{2}}} + \frac{(\mathbf{x}^p)^\dagger \mathbf{z}_b^p}{\sqrt{\frac{\sigma_w^2}{2} n_p}} \right|^2. \quad (29)$$

which implies that

$$T_l \sim \chi_2^2 \left(\frac{2|\gamma_{ab}|^2 n_p P_a G_l}{\sigma_b^2} \right), \quad l \in [1 : L], \quad (30)$$

by the definition of noncentral chi-squared distribution, where *i*) when Alice and Bob's beams are perfectly aligned, $G_l = W_a F_b$; *ii*) when one-sided misalignment occurs at Alice or Bob side, $G_l = w_a F_b$ or $G_l = W_a f_b$, respectively; *iii*) when misalignment occurs at both Alice and Bob, $G_l = w_a f_b$. Moreover, these variables are independent, since they are constructed from training measurements at different time. ■

For ease of exposition and without loss of generality, we further assume that variables $\{T_2, \dots, T_{L_a+1}\} \sim \chi_2^2(\lambda_B)$, $\{T_{L_a+2}, \dots, T_{L_a+L_b+1}\} \sim \chi_2^2(\lambda_C)$ and $\{T_{L_a+L_b+2}, \dots, T_L\} \sim \chi_2^2(\lambda_D)$. We now establish a lower bound on p_{align} as stated in the following proposition.

Proposition 1: The probability of successful alignment p_{align} is lowered bound by p_{LB} :

$$p_{\text{LB}}(P_a, n_p) = 1 - p_{\text{miss},1} - p_{\text{miss},2} - p_{\text{miss},3}, \quad (31)$$

where

$$p_{\text{miss},1} = 1 - \int_0^\infty (F(t|2, \lambda_B))^{L_a-1} f(t|2, \lambda_A) dt, \quad (32)$$

$$p_{\text{miss},2} = 1 - \int_0^\infty (F(t|2, \lambda_C))^{L_b-1} f(t|2, \lambda_A) dt, \quad (33)$$

$$p_{\text{miss},3} = 1 - \int_0^\infty (F(t|2, \lambda_D))^{(L_a-1)(L_b-1)} f(t|2, \lambda_A) dt, \quad (34)$$

with $f(t|k, \lambda)$ and $F(t|k, \lambda)$ being the probability density function (pdf) and the cumulative distribution function (cdf) of $\chi_k^2(\lambda)$, respectively.

Proof: The proof uses the definition of p_{align} as in (24) and the statistical properties of the random variables established in Lemma 1. The details are deferred to Appendix A. ■

Based on this proposition and from (21), the approximated \bar{T} is lowered bound by \bar{T}_{LB} given by:

$$\begin{aligned} \bar{T}_{\text{LB}} &= \left(1 - \frac{n_a}{n}\right) \log \left(1 + \frac{P_d |\gamma_{ab}|^2}{\sigma_b^2} W_a F_b\right) p_{\text{LB}}(P_a, n_p) \\ &= \left(1 - \frac{n_p L}{n}\right) \log \left(1 + \frac{P_d |\gamma_{ab}|^2}{\sigma_b^2} W_a F_b\right) p_{\text{LB}}(P_a, n_p). \end{aligned} \quad (35)$$

B. Detection Performance at Willie

As for Willie, let \mathbb{P}_0 and \mathbb{P}_1 be the probability distribution of its observations under \mathcal{H}_0 and \mathcal{H}_1 as in (15), respectively. In particular, under \mathcal{H}_0 , the distribution \mathbb{P}_0 is given by:

$$\mathbb{P}_0 = \frac{1}{(\pi \sigma_w^2)^n} \exp \left(-\frac{\sum_{i=1}^n |y_w^i|^2}{\sigma_w^2} \right), \quad (36)$$

since only noises are observed at Willie. Under \mathcal{H}_1 , the distribution \mathbb{P}_1 can be represented by:

$$\mathbb{P}_1 = \mathbb{P}_1^{\text{BA}} \times \mathbb{P}_1^{\text{DT}}, \quad (37)$$

where \mathbb{P}_1^{BA} corresponds to the joint distribution of received signals at Willie when Alice and Bob are in the BA phase, while \mathbb{P}_1^{DT} corresponds to the joint distribution of received signals at Willie when Alice and Bob are in the DT phase. Considering that Willie has no knowledge of the pilot sequence used for beam training between Alice and Bob, based on (15) and (17), \mathbb{P}_1^{BA} is approximately characterized by

$$\begin{aligned} \mathbb{P}_1^{\text{BA}} &= \frac{1}{(\pi(\sigma_w^2 + |\gamma_{aw}|^2 P_a W_a))^{L_b n_p}} \exp \left(-\frac{\sum_{i=1}^{n_p} |y_w^i|^2}{\sigma_w^2 + |\gamma_{aw}|^2 P_a W_a} \right) \\ &\times \frac{1}{(\pi(\sigma_w^2 + |\gamma_{aw}|^2 P_a w_a))^{L_b (L_a - 1) n_p}} \exp \left(-\frac{\sum_{i=n_p+1}^{n_a} |y_w^i|^2}{\sigma_w^2 + |\gamma_{aw}|^2 P_a w_a} \right). \end{aligned} \quad (38)$$

To characterize \mathbb{P}_1^{DT} , we note from (18) that Willie's received signals would depend on whether it is in the main-lobe or in the side-lobe of Alice's chosen beam for data transmission. To account for this factor, let ρ be the probability that Willie is in the main-lobe of Alice's data beam. Then \mathbb{P}_1^{DT} can be characterized by a mixture of $\mathbb{P}_{1,1}^{\text{DT}}$ and $\mathbb{P}_{1,2}^{\text{DT}}$ as

$$\mathbb{P}_1^{\text{DT}} = \rho \mathbb{P}_{1,1}^{\text{DT}} + (1 - \rho) \mathbb{P}_{1,2}^{\text{DT}}, \quad (39)$$

where we have

$$\begin{aligned} \mathbb{P}_{1,1}^{\text{DT}} &= \frac{1}{(\pi(\sigma_w^2 + |\gamma_{aw}|^2 P_d W_a))^{n - n_a}} \exp \left(-\frac{\sum_{i=n_a+1}^n |y_w^i|^2}{\sigma_w^2 + |\gamma_{aw}|^2 P_d W_a} \right), \\ \mathbb{P}_{1,2}^{\text{DT}} &= \frac{1}{(\pi(\sigma_w^2 + |\gamma_{aw}|^2 P_d w_a))^{n - n_a}} \exp \left(-\frac{\sum_{i=n_a+1}^n |y_w^i|^2}{\sigma_w^2 + |\gamma_{aw}|^2 P_d w_a} \right), \end{aligned}$$

as the joint probability distribution of Willie's received signals when it is in the main-lobe and in the side-lobe of Alice's data beam, respectively.

Based on the \mathbb{P}_0 and \mathbb{P}_1 computed, Willie performs a binary hypothesis testing. It is known that the error probability that

Willie can be achieved is lower bounded by:

$$\xi^* = 1 - \nu_T(\mathbb{P}_0, \mathbb{P}_1), \quad (40)$$

where $\nu_T(\mathbb{P}_0, \mathbb{P}_1)$ is the total variation distance between \mathbb{P}_0 and \mathbb{P}_1 . However, the closed-form expression of this total variation is hard to obtain for the given \mathbb{P}_0 and \mathbb{P}_1 in our case. Alternatively, as in many existing works [2], [6], [8], we consider the following upper bound on the total variation by using Pinsker's inequality [32]:

$$\nu_T(\mathbb{P}_0, \mathbb{P}_1) \leq \sqrt{\frac{1}{2} \mathcal{D}(\mathbb{P}_0 || \mathbb{P}_1)} \quad (41)$$

where $\mathcal{D}(\mathbb{P}_0 || \mathbb{P}_1)$ is the relative entropy of \mathbb{P}_0 to \mathbb{P}_1 defined by:

$$\mathcal{D}(\mathbb{P}_0 || \mathbb{P}_1) = \int p_0(x) \ln \frac{p_0(x)}{p_1(x)} dx. \quad (42)$$

As a result, a sufficient condition to ensure the covertness constraint $\xi^* \geq 1 - \epsilon$ at Willie is that

$$\mathcal{D}(\mathbb{P}_0 || \mathbb{P}_1) \leq 2\epsilon^2. \quad (43)$$

We further note that \mathbb{P}_1 in our case contains a mixture of multivariate Gaussian component \mathbb{P}_1^{DT} as in (39), which renders closed-form expression for $\mathcal{D}(\mathbb{P}_0 || \mathbb{P}_1)$ still difficult. To make the problem more tractable, we further approximate \mathbb{P}_1^{DT} by a joint distribution $\bar{\mathbb{P}}_1^{\text{DT}}$ as given by

$$\bar{\mathbb{P}}_1^{\text{DT}} = \frac{1}{(\pi(\sigma_w^2 + |\gamma_{aw}|^2 P_d \bar{w}_a))^{n-n_a}} \exp\left(-\frac{\sum_{i=n_a+1}^n |y_w^i|^2}{\sigma_w^2 + |\gamma_{aw}|^2 P_d \bar{w}_a}\right), \quad (44)$$

whose underlying variables are i.i.d. Gaussian distributed with zero mean and variance $(\sigma_w^2 + |\gamma_{aw}|^2 P_d \bar{w}_a)$ with $\bar{w}_a = \rho W_a + (1 - \rho)w_a$. Namely, we approximate each underlying mixture Gaussian variable in \mathbb{P}_1^{DT} of (39) with a single Gaussian variable of the same mean and variance. Letting $\bar{\mathbb{P}}_1 = \mathbb{P}_1^{\text{BA}} \times \bar{\mathbb{P}}_1^{\text{DT}}$, we thus approximate $\mathcal{D}(\mathbb{P}_0 || \mathbb{P}_1)$ by $\mathcal{D}(\mathbb{P}_0 || \bar{\mathbb{P}}_1)$, which can be derived in closed-form as:

$$\begin{aligned} \mathcal{D}(\mathbb{P}_0 || \bar{\mathbb{P}}_1) &= L_b n_p \left[\ln(1 + \xi_1) - \frac{\xi_1}{1 + \xi_1} \right] \\ &+ L_b (L_a - 1) n_p \left[\ln(1 + \xi_2) - \frac{\xi_2}{1 + \xi_2} \right] \\ &+ (n - n_a) \left[\ln(1 + \xi_3) - \frac{\xi_3}{1 + \xi_3} \right], \end{aligned} \quad (45)$$

with $\xi_1 = |\gamma_{aw}|^2 P_a W_a / \sigma_w^2$, $\xi_2 = |\gamma_{aw}|^2 P_a w_a / \sigma_w^2$ and $\xi_3 = |\gamma_{aw}|^2 P_d \bar{w}_a / \sigma_w^2$. We note that this approximation is accurate in particular when the signal-to-noise-ratio (SNR) at Willie is relatively small (a typical case in covert communications).

C. Problem Formulation

Given the lower bound \bar{T}_{LB} of (35) on the throughput of Alice-Bob link and the covertness constraint of (43) at Willie,

we formulate the following optimization problem in our covert communication design:

$$\max_{P_a, P_d, n_p} \left(1 - \frac{n_p L}{n}\right) \log \left(1 + \frac{P_d |\gamma_{ab}|^2}{\sigma_b^2} W_a F_b\right) p_{\text{LB}}(P_a, n_p) \quad (46a)$$

$$\text{s.t. } \mathcal{D}(\mathbb{P}_0 || \bar{\mathbb{P}}_1) \leq 2\epsilon^2, \quad (46b)$$

$$1 \leq n_p \leq \left\lfloor \frac{n}{L} \right\rfloor, n_p \in \mathbb{N}, \quad (46c)$$

which aims to optimize the number of symbols n_p allocated to each beam pair trained ($n_p L$ thus reflects the total training overhead), training power P_a and data transmission power P_d in order to maximize \bar{T}_{LB} , subject to the covertness constraint at Willie.

It is noted that while optimizing lower bound \bar{T}_{LB} might not give exactly the same results as optimizing the true effective throughput, this problem still provides valuable insights into the tradeoff between beam training overhead and achievable rate for Alice-Bob link, and also the tradeoff between the rate performance of Alice-Bob link and the achievable covertness level against Willie. Specifically, spending more symbols on beam training would improve the beam alignment performance between Alice and Bob, but at the expense of reducing the time left for data transmission. In addition, having larger training power and data transmission power would improve the effective throughput of Alice-Bob link, but at the risk of violating the covertness constraint imposed on Willie.

Solving problem (46) is quite challenging because the optimization variables are coupled in the nonconvex objective function and constraints. Moreover, the training overhead for each beam pair n_p is a discrete variable, which further complicates the solution of problem (46). Hence, we are faced with a mixed-integer nonlinear programming problem, which is usually considered as NP-hard. In principle, one can attempt to perform exhaustive search over variable space (n_p, P_a, P_d) to find the optimal solution, but this would require traversing all possible n_p values and proper discretization of (P_a, P_d) , which leads to extremely high computational complexity and an unaffordable computation overhead. In the next section, we shall propose a more efficient algorithm to solve this problem.

IV. DUAL-DECOMPOSITION SUCCESSIVE CONVEX APPROXIMATION ALGORITHM

In this section, we develop an efficient double-loop iterative algorithm named DSCA, which integrates dual-decomposition [33] with successive convex approximation (SCA) method [34] to find the stationary solution of problem (46). Specifically, we first recast problem (46) into a more tractable yet equivalent form by exploiting its structural properties. We then elaborate the design of the proposed algorithm and also prove its convergence to a local stationary point.

$$f(\theta) = \log \left(1 - \frac{n_p L}{n}\right) + \log p_{\text{LB}}(P_a, n_p) + \log \log \left(1 + \frac{P_d |\gamma_{ab}|^2}{\sigma_b^2} W_a F_b\right), \quad (48)$$

A. Problem Reformulation

Before proceeding to the derivation of the proposed algorithm, a suitable transformation for problem (46) is necessary, and we provide the following corollary:

Corollary 1: Problem (46) is equivalent to

$$\begin{aligned} \max_{\boldsymbol{\theta}} f(\boldsymbol{\theta}) \\ \text{s.t. (46b) - (46c)} \end{aligned} \quad (47)$$

where $\boldsymbol{\theta} \triangleq [P_a, P_d, n_p]^T$ denotes the composite optimization variable, and the objective function $f(\boldsymbol{\theta})$ is defined in (48) as displayed at the bottom of the next page.

Since the log function is monotonically nondecreasing and also analytic in the real region, Corollary 1 can be easily proved. It is noteworthy that the above equivalent transformation would facilitate the separation of optimization variables, thereby simplifying the subsequent development of the proposed algorithm.

To make the problem tractable, we subsequently relax the discrete integer constraint (46c) into a closed connected subset of the real axis, i.e., $1 \leq n_p \leq \lfloor \frac{n}{L} \rfloor$. We remark that the limiting point generated by the proposed DSCA algorithm may not satisfy the integer constraint in (46c). To obtain an integer solution for the optimal training overhead required by each beam pair, we use the same method as in [35] to round n_p to its nearby integer as follows

$$n_p(\delta) = \begin{cases} \lfloor n_p^* \rfloor, & \text{if } n_p^* - \lfloor n_p^* \rfloor \leq \delta \\ \lceil n_p^* \rceil, & \text{otherwise,} \end{cases} \quad (49)$$

where $0 \leq \delta \leq 1$ is chosen such that constraint (46b) is met. Since $D(\mathbb{P}_0 || \bar{\mathbb{P}}_1)$ is monotonic in n_p , we can always find such δ using a bisection search over $\delta \in [0, 1]$.

However, problem (47) remains to be solved due to the nonlinear coupling of variables in the covertness constraint (46b). To overcome this difficulty, we decouple problem (47) into a master dual problem and a subproblem by leveraging dual decomposition method [33]. For the problem at hand, the first step is to introduce the nonnegative Lagrange multiplier ν associated with the covertness constraint (46b) and to write the partial Lagrangian of problem (47) as

$$\mathcal{L}(\boldsymbol{\theta}, \nu) = f(\boldsymbol{\theta}) - \nu (\mathcal{D}(\mathbb{P}_0 || \bar{\mathbb{P}}_1) - 2\epsilon^2). \quad (50)$$

Then the dual function can be expressed as

$$h(\nu) = \max_{\boldsymbol{\theta}} \mathcal{L}(\boldsymbol{\theta}, \nu) \quad \text{s.t. (46b)}. \quad (51)$$

Given the fixed dual variable ν , the subproblem w.r.t. $\boldsymbol{\theta}$ can be written as

$$\max_{\boldsymbol{\theta}} f(\boldsymbol{\theta}) - \nu \mathcal{D}(\mathbb{P}_0 || \bar{\mathbb{P}}_1) \quad \text{s.t. (46b)}. \quad (52)$$

Based upon the optimal solution $\boldsymbol{\theta}^*$ to problem (52), we have the master dual problem in charge of updating the dual variable ν by solving the following problem:

$$\min_{\nu \geq 0} h(\nu) \quad (53)$$

In a nutshell, the master dual problem sets the price for the resources in each subproblem, which in turns decides the amount of used resources depending on the price [36]. In the sequel, we show how the master dual problem (53) and the subproblem (52) are efficiently solved. Hereinafter, we let superscript t denote variables associated with the t -th iteration.

B. Proposed DSCA Algorithm

1) Subgradient Method for Solving Master Dual Problem:

The Lagrangian duality theory in optimization states that the updating of the dual variable can be achieved via the minimization of $h(\nu)$, e.g., using the subgradient method [37]. Since the subgradient of h at ν is simply the covertness constraint residual $\mathcal{D}(\mathbb{P}_0 || \bar{\mathbb{P}}_1) - \epsilon^2$, (53) can be efficiently solved with the following updates

$$\nu^{t+1} = [\nu^t + \eta^t (\mathcal{D}^t(\mathbb{P}_0 || \bar{\mathbb{P}}_1) - 2\epsilon^2)]_+ \quad (54)$$

where η^t is the step size, $[\cdot]_+$ refers to the projection operation onto the nonnegative orthant, and $\mathcal{D}^t(\mathbb{P}_0 || \bar{\mathbb{P}}_1)$ is the relative entropy of \mathbb{P}_0 to $\bar{\mathbb{P}}_1$ at the current point $\boldsymbol{\theta}^t$ generated by the last iteration.

Note that since the master dual problem (53) is always convex, the subgradient method is guaranteed to converge exactly to its globally optimal solution. In addition, the convergence properties of the subgradient method heavily rely on the choice of step size sequence $\{\eta^t\}$. Constant step size is a typical choice of $\{\eta^t\}$, but different step size should be properly chosen for different covertness level $2\epsilon^2$ for better performance. In this paper we adopt the diminishing step sizes as suggested in [38].

2) *IBCD Method for Solving Subproblem:* To solve subproblem (52), we observe first that the constraints are separable with respect to the three blocks of variables, i.e., P_a , P_d , and n_p , which allows applying the inexact block coordinate descent (IBCD) method. Similar to the BCD method, the IBCD method sequentially updates each block of variables while fixing the other blocks to their previous values. Nevertheless, in the

$$g(P_a) = \log p_{\text{LB}}(P_a) - \nu L_b n_p \left[\ln(1 + \xi_1) - \frac{\xi_1}{1 + \xi_1} \right] - \nu L_b (L_a - 1) n_p \left[\ln(1 + \xi_2) - \frac{\xi_2}{1 + \xi_2} \right], \quad (56)$$

$$\begin{aligned} g(n_p) = \log \left(1 - \frac{n_p L}{n} \right) + \log p_{\text{LB}}(n_p) - \left\{ L_b \left[\ln(1 + \xi_1) - \frac{\xi_1}{1 + \xi_1} \right] \right. \\ \left. + L_b (L_a - 1) \left[\ln(1 + \xi_2) - \frac{\xi_2}{1 + \xi_2} \right] - L_a L_b \left[\ln(1 + \xi_3) - \frac{\xi_3}{1 + \xi_3} \right] \right\} \nu n_p, \end{aligned} \quad (63)$$

IBCD method, it is only required to find an inexact solution to some subproblems while keeping the objective function nondecreasing, rather than globally solving all the subproblem. For subproblem (52), this amounts to the following steps:

Step 1(Updating P_a While Fixing P_d and n_p): Let us now consider the subproblem w.r.t. P_a , which is given by

$$\max_{P_a} g(P_a) \quad (55)$$

where the objective function $g(P_a)$ is defined in (56) as displayed at the bottom of the next page. Note that we cannot obtain the optimal P_a^* by directly maximizing $g(P_a)$ due to the nonconcave objective function. To address the challenge, we first rewrite the objective function $g(P_a)$ as follows:

$$g(P_a) = g_c(P_a) + g_n(P_a), \quad (57)$$

where $g_c(P_a)$ is the concave part of original objective function $g(P_a)$ given by

$$g_c(P_a) = \nu L_b n_p \frac{\xi_1}{1 + \xi_1} + \nu L_b (L_a - 1) n_p \frac{\xi_2}{1 + \xi_2}, \quad (58)$$

and $g_n(P_a)$ is the nonconcave part of original objective function $g(P_a)$ given by

$$g_n(P_a) = \log p_{LB}(P_a) - \nu L_b n_p \ln(1 + \xi_1) - \nu L_b (L_a - 1) n_p \ln(1 + \xi_2). \quad (59)$$

Then we preserve the partial concavity of the original objective function and linearize the nonconcave part, to construct the concave surrogate function $\hat{g}^t(P_a)$, resulting in the following

$$\hat{g}^t(P_a) = g_c(P_a) + \Gamma_A^t (P_a - P_a^t) - \tau_A (P_a - P_a^t)^2, \quad (60)$$

where $\Gamma_A^t = \frac{\partial g_n^t(P_a)}{\partial P_a}$ is the partial derivative of $g_n^t(P_a)$ w.r.t. P_a , and τ_A is a positive constant so that the surrogate function $\hat{g}^t(P_a)$ is strongly concave. Therefore, finding the optimal training power at the current iteration reduces to solving the following concave optimization problem:

$$P_a^{t+1} = \arg \max_{P_a} \hat{g}^t(P_a), \quad (61)$$

which can be efficiently solved by the the convex programming toolbox CVX [37].

Here, we remark that the well-design surrogate function $\hat{g}^t(P_a)$ will help to speed up the convergence speed by preserving the structure of the original problem. In addition, the presence of proximal regularization term $\tau_A (P_a - P_a^t)^2$ would further guarantee the algorithm convergence and can be properly chosen to achieve a good tradeoff between accuracy and computational complexity [34].

Step 2(Updating n_p While Fixing P_d and P_a): Let us now consider the subproblem w.r.t. n_p , which is given by

$$\max_{1 \leq n_p \leq \lfloor \frac{n}{L} \rfloor} g(n_p) \quad (62)$$

where the objective function $g(n_p)$ is defined in (63) as displayed at the bottom of this page.

Compared with problem (56), the above problem differs in that the training budget constraint on n_p as in (46c) is also considered. Following the same approach as used for updating P_a , we first decompose objective function $g(n_p)$ into the concave and nonconcave part and subsequently enable a SCA of the original nonconvex problem as

$$\hat{g}^t(n_p) = g_c(n_p) + \Gamma_B^t (n_p - n_p^t) - \tau_B (n_p - n_p^t)^2, \quad (64)$$

where $g_c(n_p)$ is the concave part of original objective function $g(n_p)$ is defined in (65) as given at the bottom of next page. Function $g_n(n_p) = \log p_{LB}(n_p)$ is the nonconcave part of original objective function $g(n_p)$; and $\Gamma_B^t = \frac{\partial g_n^t(n_p)}{\partial n_p}$ is the partial derivative of $g_n^t(n_p)$ w.r.t. n_p ; τ_B is a positive constant so that the surrogate function $\hat{g}^t(n_p)$ is strongly concave. By applying the projection gradient method [37], the optimal n_p can be expressed as

$$n_p^{t+1} = [\hat{n}_p^t]_1^{\lfloor \frac{n}{L} \rfloor} \quad (66)$$

where $\hat{n}_p^t = \arg \max_{n_p} \hat{g}^t(n_p)$ and $[\cdot]_b^a$ refers to the projection operation onto the box feasible region $[b, a]$.

Step 3(Updating P_d While Fixing n_p and P_a): The variable P_d is updated by solving the following unconstrained optimization problem:

$$\max_{P_d} g(P_d) \quad (67)$$

where the objective function $g(P_d)$ is defined in (68) as displayed at the bottom of next page. Likewise, we tailor a surrogate function of $g(P_d)$ with the specific structure as follows:

$$\hat{g}^t(P_d) = g_c(P_d) + \Gamma_C^t (P_d - P_d^t) - \tau_C (P_d - P_d^t)^2, \quad (69)$$

where $g_c(P_d) = \log \log \left(1 + \frac{P_d |\gamma_{ab}|^2}{\sigma_b^2} W_a F_b \right) + \frac{\nu(n-n_a)\xi_3}{1+\xi_3}$ is the concave term in $g_c(P_d)$, $g_n(P_d) = -\nu(n-n_a) \ln(1 + \xi_3)$ is the rest nonconcave term, and $\Gamma_C^t = \frac{\partial g_n^t(P_d)}{\partial P_d}$ is the partial derivative of $g_n^t(P_d)$ w.r.t. P_d , and τ_C is a positive constant to be chosen.

Finding the optimal data transmission power is reduced to

$$g_c(n_p) = - \left\{ L_b \left[\ln(1 + \xi_1) - \frac{\xi_1}{1 + \xi_1} \right] + L_b (L_a - 1) \left[\ln(1 + \xi_2) - \frac{\xi_2}{1 + \xi_2} \right] - L_a L_b \left[\ln(1 + \xi_3) - \frac{\xi_3}{1 + \xi_3} \right] \right\} \nu n_p + \log \left(1 - \frac{n_p L}{n} \right), \quad (65)$$

$$g(P_d) = \log \log \left(1 + \frac{P_d |\gamma_{ab}|^2}{\sigma_b^2} W_a F_b \right) - \nu(n - n_a) \left[\ln(1 + \xi_3) - \frac{\xi_3}{1 + \xi_3} \right], \quad (68)$$

Algorithm 1: Proposed DSCA Algorithm

Initialization: Define the tolerance of accuracy ω and the maximum number of iterations T_{\max} . Let $t = 0$ and choose a feasible initial point;

repeat

- Step 1:** Update ν^t according to (54);
- Step 2:** Update P_a^t according to (61);
- Step 3:** Update n_p^t according to (66);
- Step 4:** Update P_d^t according to (70);
- Step 5:** Let $t = t + 1$;

until the increment on the value of the objective function in (50) is less than some threshold $\epsilon_2 > 0$ or reaching the maximum iteration number;

solving the following concave approximated problem:

$$P_d^{t+1} = \arg \max_{P_d} \hat{g}^t(P_d) \quad (70)$$

which can be optimally determined by the standard convex optimization method.

3) *Overall DSCA Algorithm:* According to the aforementioned results, we summarize the proposed DSCA algorithm in Algorithm 1, where Steps 2-4 correspond to the three sub-iterations of the IBCD method. In subsequent, we establish the local convergence of the proposed DSCA algorithm to stationary solutions, using the following proposition.

Proposition 2: The proposed algorithm produces non-descending objective value sequence. Moreover, any limiting point (P_a^*, n_p^*, P_d^*) generated by the DSCA algorithm is a KKT point of problem (46).

Proof: Refer to Appendix B for the detailed proof. ■

This proposition indicates that the proposed algorithm monotonically converges to a stationary point of problem (46). The monotonic convergence is attractive since it guarantees an improved objective value with arbitrary random initialization. In the next section, we will provide numerical results on the problem and draw insights on how much training is needed for the joint design of beam alignment and data transmission in covert mmWave communication.

V. NUMERICAL RESULTS

In the simulations below, Alice has $N_a = 32$ transmit antennas and Bob has $N_b = 8$ receive antenna. Unless stated otherwise, Alice and Bob are assumed to deploy $L_a = 32$ and $L_b = 8$ generalized flat-top beams as defined in Section II-B to cover AoD and AoA $[0, 2\pi]$ range, respectively. For each beam, its main-lobe gain is assumed to be 0.5 dB lower than that of ideal flat-top beam, and thus its side-lobe gain can be determined accordingly by the law of energy conservation. Therefore, we have that

$$W_a = L_a 10^{-0.05}, \quad w_a = (2 - (2/L_a * W_a)) / (2 - 2/L_a); \quad (71)$$

$$F_b = L_b 10^{-0.05}, \quad f_b = (2 - (2/L_b * F_b)) / (2 - 2/L_b), \quad (72)$$

for Alice and Bob's beams, respectively.

Each frame is assumed to have $n = 5120$ symbols in total for beam alignment and data transmission. This frame duration is on the order of the channel coherence time for low-mobility

users in a mmWave system that operate at 73 GHz with 100-MHz bandwidth [27]. Since the total number of beam pairs to be trained is $L = L_a L_b = 256$, the number of symbols that can be spent on each beam trained is up to $n/L = 20$. As for Alice-Bob and Alice-Willie links, we define $\kappa_b \triangleq |\gamma_{ab}|^2 / \sigma_b^2$ and $\kappa_w \triangleq |\gamma_{aw}|^2 / \sigma_w^2$ as the pre-beamforming SNR, respectively, which encapsulate the path-loss of the links. Moreover, consider that Willie is chosen uniformly at random in the beam space $[-1, 1]$ and therefore the probability of Willie being in the main-lobe of Alice's data beam is $\rho = 1/L_a$ in the optimization problem (46).

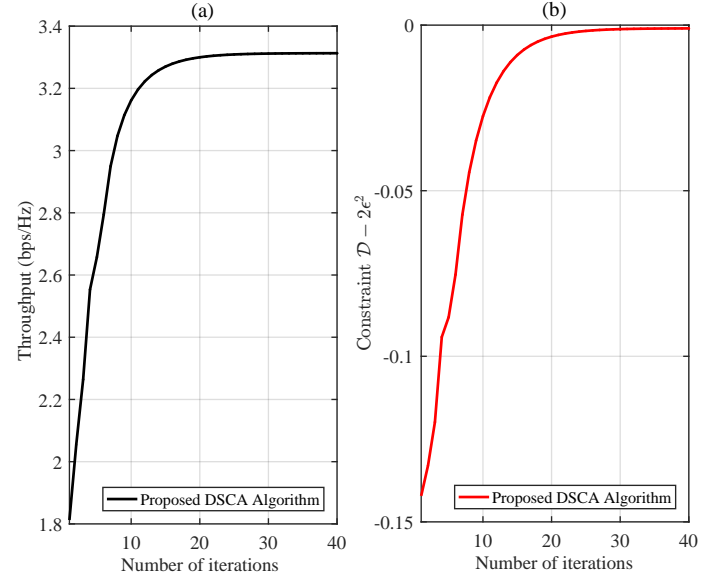


Fig. 3. Convergence behavior of the DSCA algorithm.

We first investigate the convergence behavior of the proposed DSCA algorithm. Consider that $\kappa_b = -5$ dB and $\kappa_w = -15$ dB and $\epsilon = 0.3$. Fig. 3 (a) and (b) plot an instance of the objective function and the constraint $\mathcal{D}(\mathbb{P}_0 || \mathbb{P}_1) - 2\epsilon^2$ versus the number of iterations, respectively. It can be seen that the proposed DSCA algorithm quickly converges within a few tens of iteration and the optimal solution found by the DSCA algorithm satisfies the constraint of (46b) at strict equality. This demonstrates the efficiency of the proposed algorithm.

Next, again fixing $\kappa_b = -5$ dB and $\kappa_w = -15$ dB, Fig. 4 plots the optimized \bar{T}_{LB}^* by solving (46) for different covertness levels $\epsilon \in [0.05 : 0.05 : 0.3]$ at Willie, while Fig. 5 shows the corresponding (P_a^*, P_d^*, n_p^*) that achieve \bar{T}_{LB}^* for each ϵ considered. In addition, with each (P_a^*, P_d^*, n_p^*) obtained, we also evaluate the approximate throughput \bar{T}^* in (21) by computing p_{align} via Monte-Carlo simulation and compare it against \bar{T}_{LB}^* . It can be seen that \bar{T}_{LB}^* is generally close to \bar{T}^* , which confirms the impact of the approximation in (35) is small. In general, both \bar{T}_{LB}^* and \bar{T}^* get boosted when the covertness becomes less restricted (i.e., ϵ increases). This is reasonable since larger training power and data transmission power can be used at Alice to improve the beam alignment performance and also the SNR for data transmission as ϵ increases. Another

interesting factor is that larger training power can trade fewer training symbols for each beam (see Fig. 5(b)) to maintain the same misalignment probability, thus saving more symbols/time for data transmission.

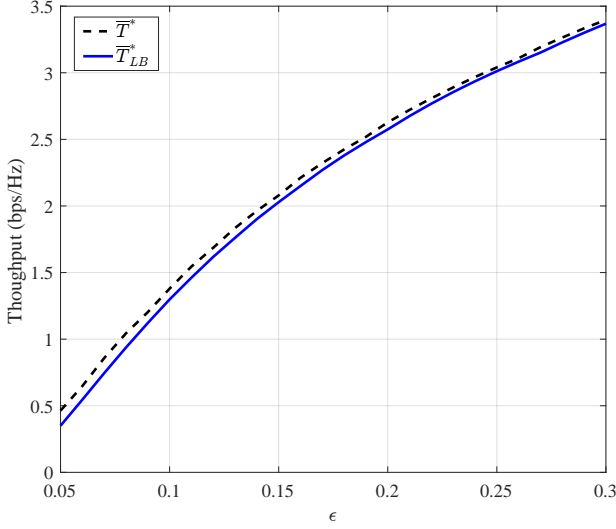


Fig. 4. Throughput versus ϵ ($\kappa_b = -5\text{dB}$, $\kappa_w = -15\text{dB}$).

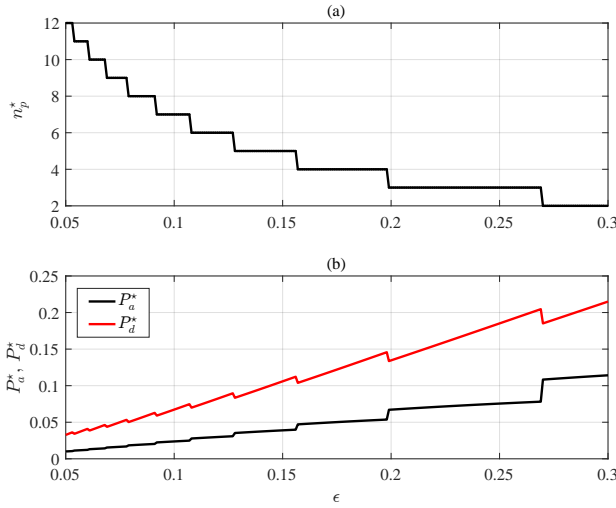


Fig. 5. The optimal (P_a^*, P_d^*, n_p^*) versus ϵ ($\kappa_b = -5\text{dB}$, $\kappa_w = -15\text{dB}$).

With $\kappa_b = -5$ dB, Fig. 6 further plots \bar{T}_{LB}^* versus κ_w under three covertness levels ($\epsilon = 0.1, 0.2, 0.3$) at Willie. In all cases, Alice-Bob link throughput drops as κ_w increases (e.g., Willie is closer to Alice). This is mainly due to the fact that training power and data transmission power at Alice have to be reduced (see Fig. 7 (a)-(b)) so as to effectively hide the communication from Willie at the covertness level required. In addition, the reduction of training power in turns requires a slight increase of symbol overhead for beam training (see Fig. 7 (c)) to maintain a reasonable alignment performance and effective throughput. This set of results again demonstrates the tradeoff among the key system design parameters and also the

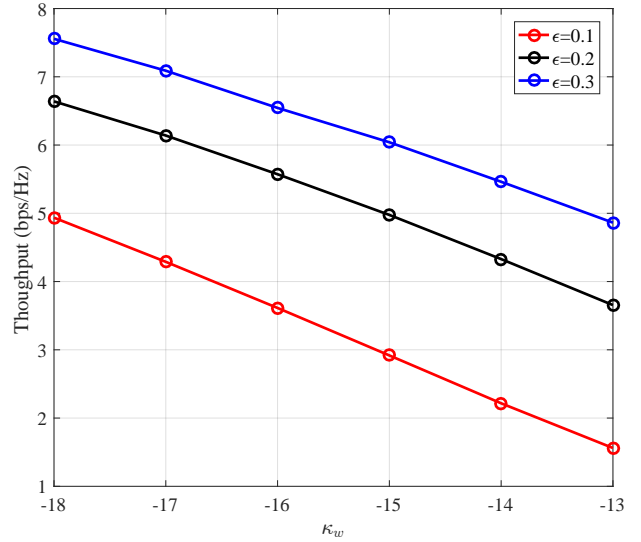


Fig. 6. Optimized \bar{T}_{LB}^* with different κ_w ($\kappa_b = -5\text{dB}$).

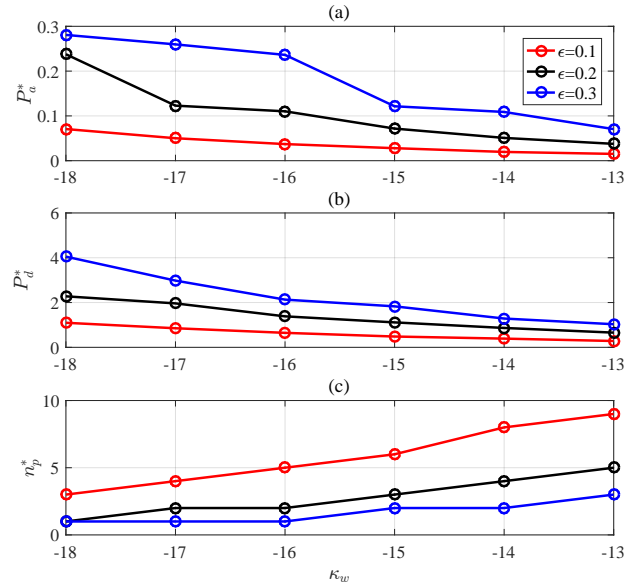


Fig. 7. The optimal (P_a^*, P_d^*, n_p^*) with different κ_w ($\kappa_b = -5\text{dB}$).

necessity of joint design of beam training and data transmission for covert mmWave communication.

We finally turn to investigate the impact of the main-lobe beamwidth of the training codebooks on the system performance. In particular, with $L_b = 8$ fixed at Bob, the number of beams at Alice L_a varies from 8 to 32, leading to more beams with narrower main-lobe beamwidth and higher beamforming gain. Having narrower beams would be beneficial for Alice-Bob link if a successful alignment can be made. However, this might increase the total training overhead as more beams need to be examined and also increase the chance of being detected when a narrow beam trained pointing towards Willie. Fig. 8 depicts the optimized \bar{T}_{LB}^* versus L_a with $\kappa_b = -5$ dB and $\kappa_w = -15$ dB. It can be seen that when the covertness requirement at Willie

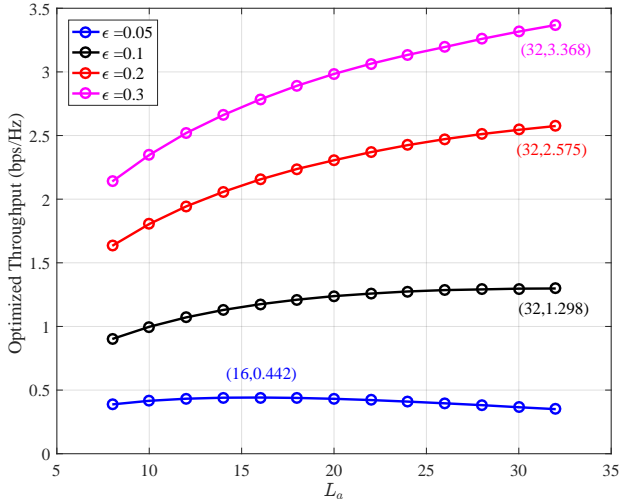


Fig. 8. Optimized \bar{T}_{LB}^* versus L_a ($\kappa_b = -5\text{dB}$, $\kappa_w = -15\text{dB}$).

is not that stringent (e.g., $\epsilon = 0.1, 0.2$ or 0.3), narrow-beam codebook with $L_a = 32$ achieves the largest throughput. On the other hand, when the covertness requirement is high, the largest throughput is attained by relatively wide-beam codebook instead, e.g., codebook with $L_a = 16$ beams only for $\epsilon = 0.05$.

VI. CONCLUSIONS

In this paper, we have considered the joint design of beam training and data transmission for a covert mmWave communication system. In particular, we have developed a framework of jointly optimizing the beam training duration, training power and data transmission power to maximize the throughput of Alice-Bob link while ensuring the covertness constraint at Willie is met. Our analytical and numerical studies have demonstrated interesting tradeoff between the legitimate link's throughput performance and the achievable covertness level against Willie, which thus lead to important guidelines on the design and optimization of covert mmWave communication. As future work, practical beam codebooks at the multi-antenna parties and more sophisticated channel models can be incorporated into the framework and their impacts on the performance of such a covert mmWave system can be examined. Moreover, it is also of great interest to develop some advanced covert beam training strategies that can further reduce the training overhead and boost the covert rate for the legitimate link.

APPENDIX A PROOF OF PROPOSITION 1

Recalling from (24), p_{align} is represented as:

$$p_{\text{align}} = 1 - \Pr\{T_1 \leq \max\{T_2, T_3, \dots, T_L\}\}, \quad (73)$$

where $\Pr\{T_1 \leq \max\{T_2, T_3, \dots, T_L\}\}$ corresponds to the probability of misalignment (denoted by p_{miss}) for Alice-Bob link. To establish a lower bound on p_{align} , we can derive an upper bound on p_{miss} . In particular, we note that

$$p_{\text{miss}} = \Pr\{T_1 \leq \max\{T_2, T_3, \dots, T_L\}\}$$

$$\begin{aligned} &= \Pr \left\{ \begin{array}{l} T_1 \leq \max\{T_2, T_3, \dots, T_{L_a+1}\}, \\ \text{or } T_1 \leq \max\{T_{L_a+2}, T_{L_a+3}, \dots, T_{L_a+L_b+1}\}, \\ \text{or } T_1 \leq \max\{T_{L_a+L_b+2}, T_{L_a+L_b+3}, \dots, T_L\} \end{array} \right\} \\ &\leq \Pr\{T_1 \leq \max\{T_2, T_3, \dots, T_{L_a+1}\}\} \\ &\quad + \Pr\{T_1 \leq \max\{T_{L_a+2}, T_{L_a+3}, \dots, T_{L_a+L_b+1}\}\} \\ &\quad + \Pr\{T_1 \leq \max\{T_{L_a+L_b+2}, T_{L_a+L_b+3}, \dots, T_L\}\} \quad (74) \\ &\triangleq p_{\text{miss},1} + p_{\text{miss},2} + p_{\text{miss},3}, \end{aligned}$$

where (74) follows from the union bound. Moreover, by Lemma 1 and the discussions thereafter, we have that variable $T_1 \sim \chi_2^2(\lambda_A)$, while variables $\{T_2, \dots, T_{L_a+1}\} \sim \chi_2^2(\lambda_B)$, $\{T_{L_a+2}, \dots, T_{L_a+L_b+1}\} \sim \chi_2^2(\lambda_C)$ and $\{T_{L_a+L_b+2}, \dots, T_L\} \sim \chi_2^2(\lambda_D)$. Therefore, $p_{\text{miss},1}$ can be evaluated as

$$\begin{aligned} p_{\text{miss},1} &= \Pr\{T_1 \leq \max\{T_2, T_3, \dots, T_{L_a+1}\}\} \\ &= 1 - \Pr\{T_1 > \max\{T_2, T_3, \dots, T_{L_a+1}\}\} \quad (75) \end{aligned}$$

$$= 1 - \Pr\{T_2 < T_1, T_3 < T_1, \dots, T_{L_a+1} < T_1\} \quad (76)$$

$$= 1 - \int_0^\infty (F(t|2, \lambda_B))^{L_a-1} f(t|2, \lambda_A) dt, \quad (77)$$

where $f(t|k, \lambda)$ and $F(t|k, \lambda)$ are the pdf and cdf of $\chi_k^2(\lambda)$, respectively. The other two terms $p_{\text{miss},2}$ and $p_{\text{miss},3}$ can be evaluated similarly. In this way, we establish an upper bound on p_{miss} as $p_{\text{miss}} \leq p_{\text{miss},1} + p_{\text{miss},2} + p_{\text{miss},3}$, which leads to a lower bound on p_{align} as $p_{\text{align}} \geq p_{LB} = 1 - p_{\text{miss},1} - p_{\text{miss},2} - p_{\text{miss},3}$.

APPENDIX B PROOF OF PROPOSITION 2

We first prove the existence of at least one limiting point before stating that any limiting point generated by Algorithm 1 is a stationary solution. In this paper, the feasible set of each variable block is compact, respectively. In addition, the problem (46) over the feasible region is bounded. Hence, the sequence of iterates P_a^t, n_p^t, P_d^t generated by Algorithm 1 is compact and bounded. Since any compact and bounded sequence must have at least one limiting point, the existence of a limiting point of Algorithm 1 is guaranteed.

Let $\theta^* \triangleq (P_a^*, P_d^*, n_p^*)$ and ν^* be the primal and dual optimal points generated by Algorithm 1. For convenience, the KKT conditions for problem (47) are elaborated below:

$$\begin{aligned} \nabla f(\theta^*) + \nu^* (\mathcal{D}^t(\mathbb{P}_0 || \bar{\mathbb{P}}_1)(\theta^*) - 2\epsilon^2) &= 0, \\ \nu^* (\mathcal{D}^t(\mathbb{P}_0 || \bar{\mathbb{P}}_1)(\theta^*) - 2\epsilon^2) &= 0, \\ \mathcal{D}^t(\mathbb{P}_0 || \bar{\mathbb{P}}_1)(\theta^*) - 2\epsilon^2 &\leq 0, \nu^* \geq 0. \end{aligned}$$

All these conditions follows immediately from the fact that the surrogate functions designed in the Algorithm 1 satisfy the function value consistency, gradient consistency and lower bound conditions defined in [34], which can be easily verified. Consequently, we can conclude that the objective function value is nondecreasing after each iteration. Therefore, the limiting point θ^* is a KKT point of problem (47). Note that (46) and (47) are equivalent, in the sense that the optimal solution θ^* for the two problems are identical. This concludes that the limiting point produced by Algorithm 1 is a KKT point of problem (46). This completes the proof.

REFERENCES

- [1] B. A. Bash, D. Goeckel, D. Towsley, and S. Guha, "Hiding information in noise: Fundamental limits of covert wireless communication," *IEEE Commun. Mag.*, vol. 53, no. 12, pp. 26–31, 2015.
- [2] B. A. Bash, D. Goeckel, and D. Towsley, "Limits of reliable communication with low probability of detection on AWGN channels," *IEEE J. Select. Areas Commun.*, vol. 31, no. 9, pp. 1921–1930, 2013.
- [3] Z. Liu, J. Liu, Y. Zeng, and J. Ma, "Covert wireless communications in IoT systems: Hiding information in interference," *IEEE Wireless Commun.*, vol. 25, no. 6, pp. 46–52, 2018.
- [4] S. Yan, X. Zhou, J. Hu, and S. V. Hanly, "Low probability of detection communication: Opportunities and challenges," *IEEE Wireless Commun.*, vol. 26, no. 5, pp. 19–25, 2019.
- [5] P. H. Che, M. Bakshi, and S. Jaggi, "Reliable deniable communication: Hiding messages in noise," in *Proc. IEEE Int. Symp. Inf. Theory, Istanbul, Turkey, Jul. 2013.*, pp. 2945–2949.
- [6] L. Wang, G. W. Wornell, and L. Zheng, "Fundamental limits of communication with low probability of detection," *IEEE Trans. Inform. Theory*, vol. 62, no. 6, pp. 3493–3503, 2016.
- [7] T. V. Sobers, B. A. Bash, S. Guha, D. Towsley, and D. Goeckel, "Covert communication in the presence of an uninformed jammer," *IEEE Trans. Wireless Commun.*, vol. 16, no. 9, pp. 6193–6206, 2017.
- [8] S. Yan, B. He, X. Zhou, Y. Cong, and A. L. Swindlehurst, "Delay-intolerant covert communications with either fixed or random transmit power," *IEEE Trans. Inf. Forensics Security.*, vol. 14, no. 1, pp. 129–140, 2018.
- [9] S. Yan, Y. Cong, S. V. Hanly, and X. Zhou, "Gaussian signalling for covert communications," *IEEE Trans. Wireless Commun.*, vol. 18, no. 7, pp. 3542–3553, 2019.
- [10] K. Shahzad, X. Zhou, and S. Yan, "Covert communication in fading channels under channel uncertainty," in *Proc. IEEE Vehicular Technol. Conf. Spring, Jun. 2017.*, pp. 1–5.
- [11] T. Xu, L. Sun, S. Yan, J. Hu, and F. Shu, "Pilot-based channel estimation design in covert wireless communication," 2019, *arXiv:1908.00226*. [Online] Available <https://arxiv.org/abs/1908.00226v1>.
- [12] B. He, S. Yan, X. Zhou, and V. K. Lau, "On covert communication with noise uncertainty," *IEEE Commun. Lett.*, vol. 21, no. 4, pp. 941–944, 2017.
- [13] R. Soltani, D. Goeckel, D. Towsley, B. A. Bash, and S. Guha, "Covert wireless communication with artificial noise generation," *IEEE Trans. Wireless Commun.*, vol. 17, no. 11, pp. 7252–7267, 2018.
- [14] S. Lee, R. J. Baxley, J. B. McMahon, and R. S. Frazier, "Achieving positive rate with undetectable communication over MIMO rayleigh channels," in *Proc. IEEE 8th Sensor Array Multichannel Signal Process. Workshop, Jun. 2014.*, pp. 257–260.
- [15] A. Abdelaziz and C. E. Koksal, "Fundamental limits of covert communication over MIMO AWGN channel," in *Proc. IEEE Conf. Commun. Netw. Secur., Las Vegas, NV, USA, Oct. 2017.*, pp. 1–9.
- [16] T.-X. Zheng, H.-M. Wang, D. W. K. Ng, and J. Yuan, "Multi-antenna covert communications in random wireless networks," *IEEE Trans. Wireless Commun.*, vol. 18, no. 3, pp. 1974–1987, 2019.
- [17] J. Hu, Y. Wu, R. Chen, F. Shu, and J. Wang, "Optimal detection of UAV's transmission with beam sweeping in covert wireless networks," *IEEE Trans. Veh. Technol.*, 2019.
- [18] K. Shahzad, X. Zhou, and S. Yan, "Covert wireless communication in presence of a multi-antenna adversary and delay constraints," *IEEE Trans. Veh. Technol.*, vol. 68, no. 12, pp. 12432–12436, 2019.
- [19] K. Shahzad, X. Zhou, S. Yan, J. Hu, F. Shu, and J. Li, "Achieving covert wireless communications using a full-duplex receiver," *IEEE Trans. Wireless Commun.*, vol. 17, no. 12, pp. 8517–8530, 2018.
- [20] K. S. K. Arumugam, M. R. Bloch, and L. Wang, "Covert communication over a physically degraded relay channel with non-colluding wardens," in *Proc. IEEE Int. Symp. Inf. Theory (ISIT), Vail, CO, USA, Jun. 2018.*, pp. 766–770.
- [21] J. Wang, W. Tang, Q. Zhu, X. Li, H. Rao, and S. Li, "Covert communication with the help of relay and channel uncertainty," *IEEE Wireless Commun. Lett.*, vol. 8, no. 1, pp. 317–320, 2018.
- [22] J. Hu, S. Yan, F. Shu, and J. Wang, "Covert transmission with a self-sustained relay," *IEEE Trans. Wireless Commun.*, vol. 18, no. 8, pp. 4089–4102, 2019.
- [23] M. Xiao, S. Mumtaz, Y. Huang, L. Dai, Y. Li, M. Matthaiou, G. K. Karagiannidis, E. Björnson, K. Yang, I. Chih-Lin *et al.*, "Millimeter wave communications for future mobile networks," vol. 35, no. 9, pp. 1909–1935, 2017.
- [24] C. Liu, M. Li, S. V. Hanly, P. Whiting, and I. B. Collings, "Millimeter wave small cells: Base station discovery, beam alignment and system design challenges," *IEEE Wireless Commun.*, vol. 25, no. 4, pp. 40–46, 2018.
- [25] S. L. Cotton, W. G. Scanlon, and B. K. Madahar, "Millimeter-wave soldier-to-soldier communications for covert battlefield operations," *IEEE Commun. Mag.*, vol. 47, no. 10, pp. 72–81, 2009.
- [26] M. V. Jamali and H. Mahdavi, "Covert millimeter-wave communication via a dual-beam transmitter," in *Proc. IEEE Global Commun. Conf. 2019.*, pp. 1–6.
- [27] C. Liu, M. Li, S. V. Hanly, I. B. Collings, and P. Whiting, "Millimeter wave beam alignment: Large deviations analysis and design insights," *IEEE J. Select. Areas Commun.*, vol. 35, no. 7, pp. 1619–1631, July 2017.
- [28] M. Li, C. Liu, S. V. Hanly, I. B. Collings, and P. Whiting, "Explore and eliminate: Optimized two-stage search for millimeter-wave beam alignment," *IEEE Trans. Wireless Commun.*, vol. 18, no. 9, pp. 4379–4393, 2019.
- [29] J. Wang, Z. Lan, C.-W. Pyo, T. Baykas, C.-S. Sum, M. A. Rahman, J. Gao, R. Funada, F. Kojima, H. Harada *et al.*, "Beam codebook based beamforming protocol for multi-Gbps millimeter-wave WPAN systems," *IEEE J. Select. Areas Commun.*, vol. 27, no. 8, pp. 1390–1399, 2009.
- [30] S. Hur, T. Kim, D. J. Love *et al.*, "Millimeter wave beamforming for wireless backhaul and access in small cell networks," *IEEE Trans. Commun.*, vol. 61, no. 10, pp. 4391–4403, 2013.
- [31] M. N. Kulkarni, S. Singh, and J. G. Andrews, "Coverage and rate trends in dense urban mmwave cellular networks," in *Proc. IEEE Global Commun. Conf., Dec. 2014.*, pp. 3809–3814.
- [32] I. Csiszár and J. Körner, *Information Theory: Coding Theorems for Discrete Memoryless Systems*. San Diego, CA, USA: Academic, 1981.
- [33] D. P. Palomar and M. Chiang, "A tutorial on decomposition methods for network utility maximization," *IEEE J. Sel. Areas Commun.*, vol. 24, no. 8, pp. 1439–1451, Aug. 2006.
- [34] M. Razaviyayn, "Successive convex approximation: Analysis and applications," Ph.D. dissertation, University of Minnesota, 2014.
- [35] A. Liu, X. Chen, W. Yu, V. K. N. Lau, and M.-J. Zhao, "Two-timescale hybrid compression and forward for massive MIMO aided C-RAN," *IEEE Trans. Signal Process.*, vol. 67, no. 9, pp. 2484C–2498, May 2019.
- [36] A. Tolli, H. Pennanen, and P. Komulainen, "Decentralized minimum power multi-cell beamforming with limited backhaul signaling," *IEEE Trans. Wireless Commun.*, vol. 10, no. 2, pp. 570–580, Feb 2011.
- [37] S. Boyd and L. Vandenberghe, "Convex optimization," in *Cambridge Univ. Press*, 2004.
- [38] X. Chen, A. Liu, Y. Cai, V. K. N. Lau, and M.-J. Zhao, "Randomized two-timescale hybrid precoding for downlink multicell massive MIMO systems," *IEEE Trans. Signal Process.*, vol. 67, no. 16, pp. 4152–4167, Aug. 2019.